Numerical Simulations and Experimental Results of Tensile Test Behavior of Laser Butt Welded DP980 Steels

S. K. Panda[1]
e-mail: s2panda@engmail.uwaterloo.ca

N. Sreenivasan

M. L. Kuntz

Y. Zhou

Centre for Advanced Materials Joining,
University of Waterloo,
Waterloo, ON, N2L 3G1, Canada

Laser welding of advanced high strength steels for fabrication of tailor welded blanks is of increasing interest for continued improvements in vehicle performance and safety without an increase in weight. Experimental results have shown that formability of welded dual-phase (DP) steels is significantly reduced by the formation of a softened region in the heat-affected zone (HAZ). In this study, a finite element simulation of welded DP980 samples undergoing transverse uniaxial tensile testing was used to evaluate the effects of soft zone width and strength on formability characteristics. Both the strength and the ductility of laser welded blanks decreased compared with those of unwelded blanks due to the formation of a softened outer-HAZ, where strain localization and final fracture occurred during tensile testing. The magnitude of softening and the width of the HAZ depend on the laser specific energy. It was observed from tensile test experiments and numerical simulations that both a decrease in strength and an increase in width of the softened HAZ were responsible for a decrease in the overall strength and ductility of the welded blanks. [DOI: 10.1115/1.2969256]

Keywords: laser welding, FE simulation, tensile test, strain localization

1 Introduction

The use of tailored blanks has increased steadily over the past 20 years and is expected to continue to rise above current levels [1,2]. Tailor welded blanks (TWBs) are produced by welding two or more sheets together prior to forming operations to tailor desired sheet thickness, strength, or coating properties in critical areas of the part. TWBs offer several notable benefits compared with monolithic blanks, such as reduced manufacturing costs, minimized offal, and improved dimensional control, as well as performance improvements and decreased part weight [1]. To further improve crash resistance and weight reduction, automotive manufacturers are evaluating the use of advanced high strength steels (AHSSs) in TWB applications. One type, dual-phase (DP) steel, is processed by intercritical annealing and rapid cooling to produce a continuous ductile ferrite matrix with islands of hard martensite [3]. This microstructure produces a high work hardening rate, resulting in higher ultimate tensile strength (UTS), compared with conventional high strength low-alloy (HSLA) steels with similar yield strengths (YSs). Thus, DP steels are suitable for forming operations and can be considered for TWB applications.

The predominate joining processes for TWB fabrication are laser beam welding and mash seam resistance welding, with laser welding more popular in North America [2]. Several laser sources have been used in laser blank welding, including CO_2 [2], Nd:YAG (yttrium aluminum garnet) [4,5], and high power diode lasers (HPDLs) [6,7]. The effects of laser welding on the microstructure and properties of DP steels have been discussed in previous work [8–10]. A laser beam traveling along the weld joint has the effect of a transient thermal wave moving through the material. The local structure and properties at any point within the weldment are generally determined by the thermal cycle experienced at that point, with the peak temperature decreasing with increasing distance from the weld centerline. In the fusion zone, the peak temperature is above the melting point. Just outside the fusion zone, near the fusion boundary, the peak temperature exceeds the critical temperature upon which 100% austenite forms (Ac_3). This region is called the supercritical heat-affected zone (HAZ). Further from the fusion boundary, the peak temperature is within the intercritical range, which results in austenitization of the carbon-rich martensite phases while large areas of undissolved ferrite remain unchanged. For transformable steels, including DP, the cooling rate through the range, which austenite decomposes to the final room temperature microstructure, is a critical determinant of the phases present, with the cooling rate largely dependent on the welding heat input. In laser welding of DP steels, the cooling rate is typically high enough to result in the decomposition of austenite to hard metastable phases such as martensite, bainite, and carbides. Thus, the room temperature microstructures of the fusion zone and the inner-HAZ (consisting of the supercritical and intercritical regions) consist of a higher volume fraction of hard phases than the base metal (with a resultant increase in microhardness) and together form a "hardened zone." Further from the fusion boundary the peak temperature is below Ac_1, the temperature where austenite transformation begins (i.e., subcritical); however, tempering of the metastable martensite phase occurs, resulting in an overall reduction in microhardness. This outer-HAZ forms a "softened zone," which is adjacent to the unaffected base metal.

The effects of severe property gradients in the weld region on the formability of welded blanks have been documented in the literature. Hardening in the fusion zone and inner-HAZ increases the strength of the weldment but decreases the ductility when strained in a direction parallel to the weld line [4,8,11]. Conversely, softening in the outer-HAZ results in a local strength decrease, especially in higher strength AHSS (i.e., 800–1000 MPa) with a substantial volume fraction of martensite [4,9,12]. When the loading direction is perpendicular to the weld line, lo-

[1]Corresponding author. Also at E3-3110, Department of Mechanical Engineering, University of Waterloo, 200 University Avenue West, Waterloo, ON, N2L 3G1, Canada.

Contributed by the Materials Division of ASME for publication in the JOURNAL OF ENGINERING MATERIALS AND TECHNOLOGY. Manuscript received December 31, 2007; final manuscript received July 2, 2008; published online August 26, 2008. Assoc. Editor: Hamid Garmestani.

calized strain causes failure in the softened zone at low loads and elongations [4,10,12,13]. With an increase in softening and softened zone width, the formability of TWBs has been found to decrease [9,10,12]. Both the severity of softening and the width of the soft zone are dictated by the heat input of the welding process. Hence, it is difficult to experimentally determine the influence of the individual effects.

Through the use of a finite element method (FEM) stamping simulation, it has been shown that the formability of laser welded blanks can be predicted without the production of test dies [14]. Numerical simulation is an effective tool for the clarification and confirmation of experimental observations. Saunders and Wagoner [15] used FEM to show that the formability of TWBs is related to the material thickness and strength ratio, as well as to weld ductility. The accuracy of the simulation, however, depends on the availability of accurate mechanical properties for both the base metal and the weld region. Methods for determining fusion zone and HAZ properties by comparing experimental tensile tests with simulation results have been proposed [16,17]; however, these methods are only able to predict hardened fusion zone and HAZ properties and do not provide a solution where HAZ softening is observed. Rodrigues et al. [18] used finite element simulations to evaluate the effects of a soft zone on the strength and ductility of welds in high strength steels subject to tensile testing. Their work, however, focused on thick sections in three-dimensional stress states, and for thin sheets, the problem can be simplified to two-dimensional stress states. Furthermore, they assumed mechanical properties for the hardened and softened zones that are difficult to determine in practice. Tomokiyo et al. [12] used FEM to clarify the effect of a softened HAZ on the formability of laser welded DP980 blanks. The material properties of the softened region were evaluated by mechanical testing of thermally simulated coupons. Their results showed that strain localization occurred in the softened HAZ, but they could not compare the analysis with experimental results and they did not consider the effects of varying soft zone width or degree of softening.

Among the material properties, the strain hardening coefficient (n) has the greatest effect on formability in stretch forming operations. It is a measure of the ability of the metal to resist localized strains and thus postpone the onset of necking/nonuniform deformation. A sheet with a high strain hardening coefficient has a better ability to uniformly distribute plastic strain, which leads to a higher elongation in uniaxial tensile testing. It can be observed that the n-value and elongation from a tensile test reflect the overall stretchability of a material in sheet forming [19]. Thus, a simulative tensile test is the quickest and easiest way to analyze sheet formability. This method can also be applied to welded blanks.

The objective of this study was to develop a numerical simulation approach for modeling the formability of laser welded blanks that have significant softening in the HAZ. Material properties for the hardened and softened regions were determined by comparing experimental results with a numerical analysis in uniaxial tensile testing. The effects of mechanical properties in the weld region, especially fusion zone hardening and HAZ softening, were characterized in terms of the formability and strength of the joint. This provided a clarification on the significance of the softened region in the HAZ in terms of the effects on the global deformation behavior of a tailor welded blank.

2 Experimental Procedures

2.1 Material Selection. Sheet metal selection is a critical component of vehicle design, enabling versatility and manufacturability. AHSS sheet can be stamped into inexpensive and complex components at high production rates. In this work, a DP steel with a nominal strength of 980 MPa (DP980) was selected for study because of its high strength and good ductility. The sheet thickness was 1.2 mm, with a galvanneal coating of 45 g/m^2 per side. The chemical composition of this steel is summarized in Table 1. The as-received microstructure of the DP980 used in this work exhibited a ferrite matrix with a significant volume fraction of fine martensite laths (49.4%) decorating the grain boundaries. The martensite displayed a banded morphology, with the martensite islands forming nearly continuous stringers along the rolling direction [13].

Table 1 Chemical composition (wt %) of the DP980 steel

Type of steel	C	Mn	Mo	Si	Cr	Al	B	Fe
DP980	0.135	2.1	0.35	0.05	0.15	0.45	0.007	Remaining

2.2 Laser Welding. Two identical sheets were welded together in a butt joint configuration to create a blank, with the weld line oriented perpendicular to the rolling direction. The sheets were welded using both HPDL (diode) and Nd:YAG laser power supplies. The sheets were tightly clamped in a fixture without backing. The faying surfaces were prepared by shearing, and the joints were arranged with the burred edge placed down, ensuring a tight fit-up. Argon shielding gas was supplied to the top surface at a rate of 14 l/min. The welding parameters were designed to produce full penetration welds free of defects such as porosity and cracking.

The heat input was varied with laser type and travel speed. The diode laser had a higher power but a much lower power density due to the larger spot size, limiting the welding to conduction mode heat transfer. The required welding speed to maintain full penetration was thus slower. The Nd:YAG laser power was lower; however, the spot size was smaller, which enabled keyhole mode welding at higher speeds. Keyhole mode welding is a characteristic of power sources that produce a high power density, such as Nd:YAG, CO_2, and fiber lasers. As a result, the diode laser had a higher net heat input relative to the Nd:YAG laser process, which was considered a lower heat input process.

The Nuvonyx 4 kW diode laser was mounted as the end effector of a Panasonic welding robot. The beam was rectangular in shape, with minimum dimensions of 12×0.9 mm^2. The beam had a focal length of 80 mm and was focused on the top surface of the sheet. The shielding gas was supplied at the leading edge of the laser spot. The blanks were welded within a speed range of 0.7–1.9 m/min. Welding slower than 0.7 m/min led to excessive weld size and sag, while speeds faster than 1.9 m/min resulted in partial penetration welds.

The Haas HL3006D Nd:YAG laser employed fiber optic beam delivery from a remote laser system to the delivery optics. The full power of 3 kW was used for the welding trials, and the beam size at the focal point was 0.6 mm in diameter. The focal length was 200 mm, and the beam was focused on the top surface of the sheet. Operating speeds were within the range of 1–6 m/min to obtain full penetration. Welding speeds less than 1 m/min led to a cutting of the material, and speeds above 6 m/min led to an incomplete penetration.

2.3 Microstructure and Microhardness Analysis. Weld characteristics were evaluated using metallographic examination and microhardness measurements. Sections were cut from the laser welded specimens, mounted, and polished as per standard metallographic procedures to observe the microstructure of the fusion zone and HAZ. The polished specimens were etched with a 2% nital solution (2 ml HNO_3, 98 ml ethanol) and were observed under an optical microscope. Cross-weld microhardness tests were conducted on the etched specimens along a straight line diagonally across the weld at an interval of 0.3 mm using an indenter load of 500 g and a duration of 15 s.

2.4 Tensile Testing. Subsize uniaxial tensile testing specimens were machined from both the welded blanks and the as-received parent metal with a width of 6 mm and a parallel length of 32 mm, as per ASTM E8 [20] (Fig. 1). In the case of the

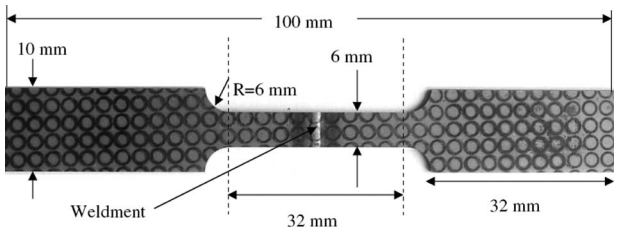

Fig. 1 Subsize tensile test specimen

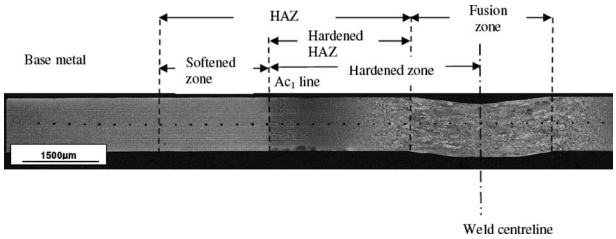

Fig. 3 Micrograph of the weldment showing different zones

welded blanks, the weld line was located at the center of the tensile specimen and was oriented perpendicular to the load direction. Tensile testing was performed using an Instron Universal Testing machine (Model 4206) at a crosshead speed of 2 mm/min.

Since the width of the fusion zone was very small in both diode and Nd:YAG laser welds, the standard ASTM E8 tensile specimen could not be used to give the tensile properties of the independent fusion zone. Longitudinal samples, which are a composite of the fusion zone, heat affected zone, and base metal properties, have been used by some [21,22] to characterize the weld metal properties. This application, however, is complicated by the presence of a softened region without known properties and cannot be used. Hence, a smaller minitensile specimen, as shown in Fig. 2, was used to obtain the mechanical properties of the fusion zone experimentally. The geometry was derived as per the tensile split Hopkinson bar (TSHB) test [23].

The HAZ exhibited steep property gradients and widths that varied with process parameters. It was impossible to prepare uniform samples for mechanical testing that represent the HAZ properties. The properties of the hard inner-HAZ were assumed to be similar to the fusion zone; however, the mechanical properties of the softened outer-HAZ could not be determined experimentally but were evaluated from the finite element analysis. Due to the heterogeneous nature of the mechanical properties across a weld, variations in strain were expected along a transverse weld tensile sample, i.e., with the weld oriented perpendicular to the load direction. Local strain in the transverse tensile sample after deformation was measured using the circular grid method. The method consisted of two stages: (i) application of uniform grids on specimens prior to deformation and (ii) visual detection to measure grid sizes at the completion of testing. A uniform circular grid was etched onto the tensile specimens by passing an alternating current through an electrolytic solution. The grid pattern was applied along the length of the tensile sample (which includes the weld and HAZ), as shown in Fig. 1. The undeformed grid size was calibrated by taking the average size of several circles. Smaller grid sizes are able to capture a higher gradient of strain in the material; hence a circular grid size of 2.0 mm diameter was used. With a grid smaller than 2.0 mm, it is expected that the shape and size become increasingly inconsistent. After the tensile test was complete, the deformed elliptical grids were measured to calculate the major strain along the length of the specimen and to obtain a strain distribution.

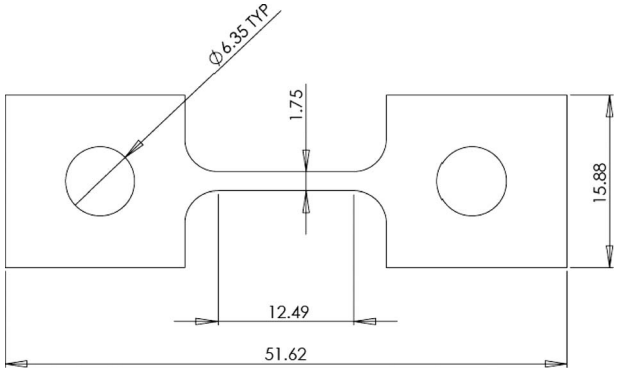

Fig. 2 Minitensile specimen used to determine the properties of weld (all dimensions are in mm)

3 Finite Element Simulation

3.1 Theoretical Background. The transverse weld specimen was a heterogeneous structure with different material properties across the various regions of the weldment, such as fusion zone, inner- and outer-HAZ, and base metal (Fig. 3). Figure 4(*a*) shows the measured cross-weld microhardness profiles for typical diode and Nd:YAG welds. The profile was relatively flat across the fusion zone with an average fusion zone hardness of $413H_V$ and $429H_V$ in the respective diode and Nd:YAG welded samples. The inner-HAZ near the fusion boundary also exhibited high hardness, decreasing toward the unaffected base metal. A softened zone was observed in the outer-HAZ where the hardness was significantly lower than the base metal. Figure 4(*b*) depicts a schematic overview of half the symmetrical tensile test sample with three different zones within the gauge length, where l_1^0, l_2^0, and l_3^0 are the initial lengths of the hardened zone (i.e., fusion zone and inner-HAZ), the initial length of the softened zone (outer-HAZ), and the initial length of the base metal, respectively. The final length of each region will be different not only due to the different initial length of each region but also due to differences in strain in the individual weld regions during deformation. The final length of the above regions after plastic deformation was defined as l_1, l_2,

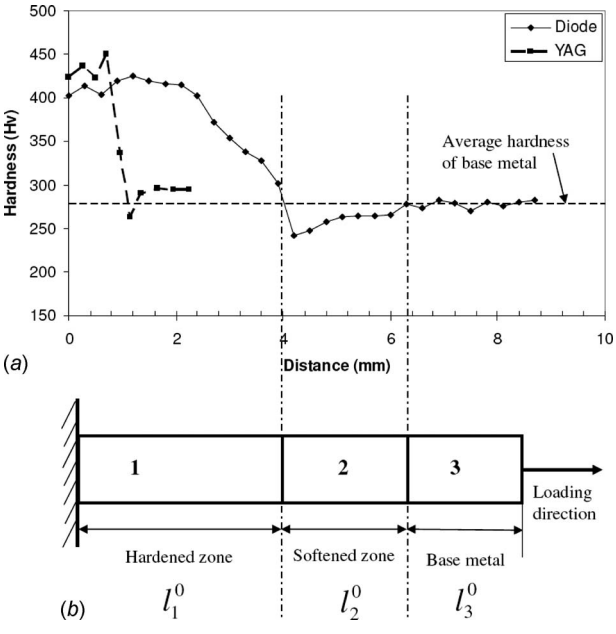

Fig. 4 Formation of three different zones in laser welding: (*a*) cross-weld hardness profiles and (*b*) schematic representation of three different zones in a transverse tensile test

and l_3, respectively.

The initial total length of the sample is represented as

$$l_0 = l_1^0 + l_2^0 + l_3^0 \tag{1}$$

and the final length as

$$l = l_1 + l_2 + l_3 \tag{2}$$

The total true strain is given as

$$\varepsilon^e = \ln\frac{l}{l_0} = \ln\frac{(l_1 + l_2 + l_3)}{(l_1^0 + l_2^0 + l_3^0)} \tag{3}$$

Since stress is assumed uniform along the sample, each zone is governed by its own constitutive equation,

$$K_1\varepsilon_1^{n_1} = K_2\varepsilon_2^{n_2} = K_3\varepsilon_3^{n_3} = \sigma \tag{4}$$

where K_1 and n_1, K_2 and n_2, and K_3 and n_3 are the strength coefficients and strain hardening exponents of the hardened zone, softened zone, and base metal, respectively. As the cross-sectional area is initially the same in all regions, the stress will initially be uniform throughout the sample. However, due to differences in mechanical properties (K- and n-values), each region will undergo different deformations, which will lead to nonuniform strain.

For each zone the strain will be as follows:

$$\varepsilon_i^e = \ln\frac{l_i}{l_i^0} \quad \text{where} \quad i = 1 - 3 \tag{5}$$

Using Eqs. (3)–(5), we get

$$\varepsilon^e = \ln\frac{l}{l_0} = \ln\left(\frac{e^{(\sigma/K_1)^{1/n_1}}l_1^0 + e^{(\sigma/K_2)^{1/n_2}}l_2^0 + e^{(\sigma/K_3)^{1/n_3}}l_3^0}{l_1^0 + l_2^0 + l_3^0}\right) \tag{6}$$

From this equation, it can be understood that the displacement and force developed in each region is governed by its strength coefficient, strain hardening exponent, and initial length. Hence, with a FEM simulation of the heterogeneous transverse weld specimen, the effect of the strength and size of the HAZ on overall mechanical properties can be studied.

3.2 FE Modeling. Numerical simulation of a tensile test was performed with the LS-DYNA-971 FEA software package (this solver handles material and geometrical nonlinearities in solving the quasistatic sheet metal forming process very well) [24]. The model was created and meshed by quadratic 2D shell elements using five-integration points with the help of the commercially available preprocessor called Hypermesh. Belytschko–Tsay thin shell elements were used to lower the computational time [24].

The following assumptions were used in the development of the model:

1. The transverse weld tensile sample consists of three distinct zones including the hardened zone, the softened zone, and the base metal.
2. The hardened zone consists of the fusion zone and the inner-HAZ.
3. The material properties in each zone are uniform.
4. The tensile sample is symmetric about the longitudinal and transverse directions.

Each region of the tensile specimen model was joined with the adjacent region by the merging of common nodes. As the sample was symmetric in both the longitudinal and transverse directions, only a quarter of the whole sample was modeled. The weld center (seam) coincided with the transverse symmetrical line. The solution domain was discretized by 5263 quadrilateral shell elements. A refined mesh was used in the weld and HAZ areas to account for the rapid change in stresses in these areas (shell element dimension of 0.1×0.1 mm^2) [25].

Figure 5 shows the TWB tensile specimen along with the boundary conditions. In order for the quarter model to represent the full specimen, both X and Y constraints were imposed on the nodes along the transverse and longitudinal symmetry lines, respectively. Displacement in the X-direction was applied to the nodes at the end of the grip portion. This displacement is equal to one-half of the final displacement obtained during the tensile test.

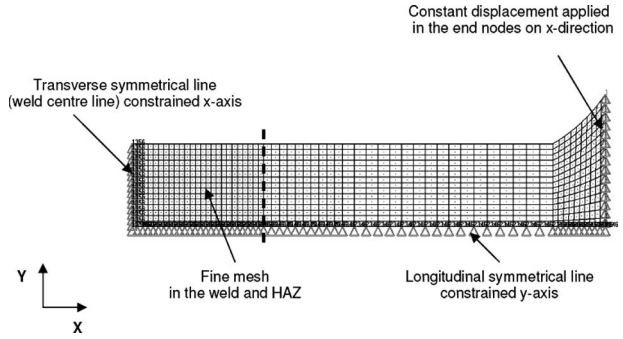

Fig. 5 FE meshes for the quarter model transverse tensile specimen with constraints in the *XY* plane

The model was considered as a deformable body with appropriate yield criterion and stress-strain relations during nonlinear plastic deformation to account for strain hardening. The yielding behavior of the blank material was considered as per the von Mises yield criterion. The simplest way to represent this criterion is $f(I_2) = I_2 = C$, where I_2 is the second invariant of the stress tensor and C is a material constant. The second invariant (I_2) of the stress tensor can be expressed in terms of the stress deviator tensor as $I_2 = (1/2)S_{ij}S_{ij}$, where, the Einstein summation convention is used. In this case, the von Mises criterion for plastic flow can be expressed as $S_{ij}S_{ij} = (2/3)\sigma_{yp}^2$, where σ_{yp} is the yield stress of the material in uniaxial tensile testing [26]. This quadratic yield condition in the Cartesian principal stress $(\sigma_1, \sigma_2, \sigma_3)$ space is represented by the following equation in terms of principal stresses:

$$\left[\frac{1}{2}\{(\sigma_1 - \sigma_2)^2 + (\sigma_2 - \sigma_3)^2 + (\sigma_3 - \sigma_1)^2\}\right]^{1/2} = \sigma_{yp} \tag{7}$$

where $\sigma_1, \sigma_2,$ and σ_3 are the principal stresses in three directions and σ_{yp} is the yield strength of the material. For a uniaxial tensile test, it can be simplified to

$$\sigma_1 = \sigma_{yp} \tag{8}$$

The stress-strain relationship during deformation was approximated by the following constitutive equation in the numerical model:

$$\sigma_y = K\varepsilon^n = K(\varepsilon_{yp} + \bar{\varepsilon}^p)^n \tag{9}$$

where σ_y=flow stress, ε_{yp}=strain to cause yield, $\bar{\varepsilon}^p$=effective plastic strain, K=strength coefficient, and n=strain hardening coefficient. This takes the nonlinear work hardening behavior of the material into account.

The elastic strain at yield can be found in [24]

$$\varepsilon_{yp} = \left[\frac{\sigma_{yp}}{K}\right]^{[1/n]} \tag{10}$$

The K- and n-values of the base metal were obtained by fitting a power law function to the true stress and true strain curve obtained from experiment. It was done by calculating the log true stress and log true strain values in the uniform plastic deformation range (between YS and UTS), and using linear regression (least squares method), a best fit was plotted. The slope of this line gives an n-value, and a Y-intercept gives log K [27].

In the case of the hardened zone, the material did not obey the power law of hardening, and the true stress and true strain curve was imported for that material model by the help of a subroutine including the stress-strain data in the program. The LS-DYNA-971 solver has the ability to evaluate stress and strain for the material

Table 2 Measured width of hardened and softened zones in laser welds

Laser	Weld speed (m/min)	Laser specific energy ($\times 10^3$ kJ/m^2)	Experimental softened zone width (mm)	Experimental hardened zone width (mm)
Diode	0.7	381	4.0	3.5
Diode	1.3	205	2.5	3.2
Diode	1.9	140	2.0	3.2
Nd:YAG	3.0	100	0.75	0.75
Nd:YAG	6.0	50	0.5	0.5

at each stage of deformation by interpolating from the data points that were imported for the stress-strain curve [24]. It was assumed that the softened HAZ obeys the power law of hardening during deformation.

As previously discussed, an experimental determination of the strength coefficient and strain hardening exponent for the HAZ was not possible. For simulation purposes, these values were obtained through a pragmatic process optimization until the load-displacement curve of the whole sample matched the experimental result (by comparing the load-displacement curve obtained from both the experiment and FE simulation, the K- and n-values were best fitted with the experimental load versus displacement curve).

4 Results and Discussion

4.1 Hardness and Microstructural Analysis. Table 2 shows the effect of welding speed, type of laser, and laser specific energy on hardened and softened zone widths (laser specific energy $=P/Vd$, where P, V, and d are laser power, welding speed, and width of the beam transverse to the welding direction, respectively). The width and hardness of the softened outer-HAZ were affected by the weld heat input. With the Nd:YAG laser, the lower heat input resulted in a narrow softened zone and a small drop in hardness. The high heat input of the diode laser produced a wider and more severe softening effect. With the significant increase in the welding speed employed when using the Nd:YAG laser, the width and degree of softening were both reduced compared with those when using the diode laser. This is due to the difference in the beam dimension transverse to the welding direction (d $=0.9$ mm and 0.6 mm for diode and Nd:YAG laser beam, respectively) and the welding speed, which together influence the laser specific energy. The width and hardness of the softened zone were also affected by the change in welding mode from a conduction to a keyhole mode for the diode and Nd:YAG power sources, respectively. This agrees with the hardness results in which the minimum hardness was lower in the diode laser welds than in the Nd:YAG welds (Fig. 4(a)).

4.2 Tensile Testing. The standard tensile properties of 0.2% offset YS, UTS, percent elongation, strain hardening coefficient (n), and strength coefficient (K) for the DP980 base metal and fusion zone are shown in Table 3. Results showed that the DP980 had fair strength and reasonable ductility for automobile part manufacturing. Figure 6 shows the engineering stress–engineering strain curve obtained from the tensile tests for the base metal and weld zone. Typical log σ-log ε plots for the base metal and weld zone are shown in Fig. 7. In the case of the base metal, a linear fit was successfully applied (after a 2.5% strain). The slope of this line was the n-value, and the Y-intercept was the log K-value. In the case of the weld metal, a good linear fit could not be attained, which indicated that it changed the slope (n-value) during deformation. Hence, the weld metal did not appear to obey the power law of hardening, and the strain hardening and strength coefficients could not be determined. The strength of the weld metal increased compared with that of the base metal, as indicated by the UTS and YS, which is related to the measured increase in hardness.

A comparison of the FEM simulation results with the experimental load-displacement curve for the DP980 base metal is shown in Fig. 8. The predicted and measured curves matched reasonably well with a small discrepancy in the initial portion of the curve. This was a result of the approximation of power law hardening by assigning a constant n-value throughout plastic deformation. In the measured curve, during the initial phase of plastic deformation the n-value was not constant until a strain of 2.5%. This behavior of DP steel is due to the presence of two different phases (ferrite and martensite), which localizes strain in the ferrite and results in a high initial work hardening rate [28].

Figure 9 shows representative engineering stress-strain curves from tensile testing of the base metal and the transverse welded samples [10]. The YS and UTS of the welded samples were lower than the base metal values. Furthermore, the overall specimen elongation was reduced, as necking and failure occurred in the softened HAZ in all welded specimens (Fig. 10). The Nd:YAG laser welds had higher strength and ductility (elongation) compared with the diode laser welds. This was due to a smaller softened HAZ width and a smaller drop in hardness with the Nd:YAG laser. Hence, it was observed that the transverse strength and ductility of laser welded DP980 depended on softened zone properties. To further understand the effect of softened zone characteristics, it was important to estimate the mechanical properties (K- and n-values) of the soft zone.

FE analysis of the welded samples was used to evaluate the effects of softened zone properties. The hardened zone and softened zone dimensions were taken from the experimental results and are shown in Table 2. The mechanical properties for the base metal were modeled with the experimentally obtained parameters. The material properties of the weld zone were incorporated by importing the measured true stress–true strain curve into the LS-DYNA-971 code. It was assumed that this curve was valid for all welding parameters for both diode and Nd:YAG laser welds. Table 4 gives the mechanical properties (K- and n-values) of the softened zone for the diode and Nd:YAG laser welds, respectively, obtained from curve fitting. To get the mechanical properties (K- and n-values) of the softened zone, trial input parameters were given and the output load displacement was matched with the corresponding experimental results. When the curves matched, the

Table 3 Mechanical properties of the DP980 base metal and the hardened zone in laser welds

	YS (MPa)	UTS (MPa)	Elongation (%)	Strength coefficient K (MPa)	Strain hardening coefficient n	Hardness (H_V)
Base metal (DP980)	534	980	15.2	1510	0.14	283
Hardened zone	804	1361	12.1	-	-	413–429

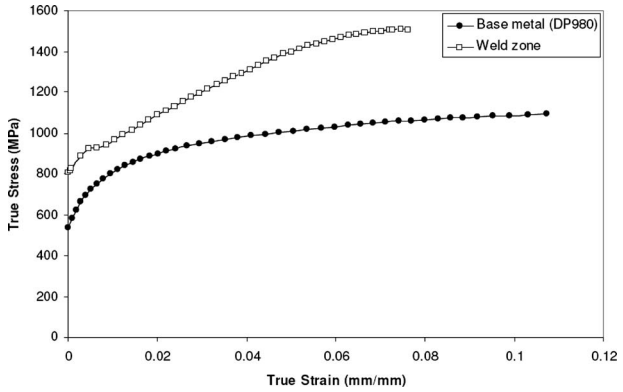

Fig. 6 True stress–true strain curve obtained from the experiment for base metal (DP980) and weld

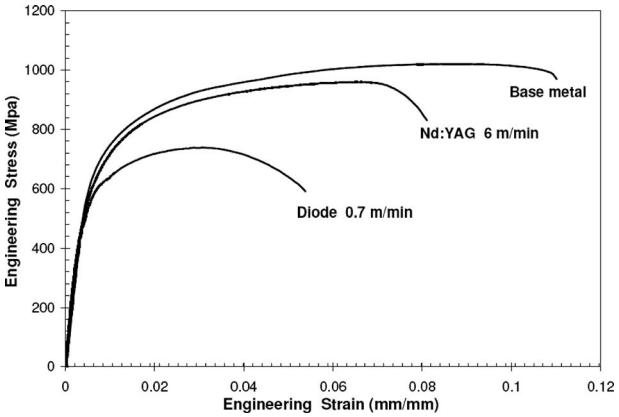

Fig. 9 Comparison of the stress-strain behaviors of the base metal and transverse welded blanks

corresponding *K*- and *n*-values were adopted as the mechanical properties of the softened HAZ. Figure 11 shows the matching of load-displacement curves obtained from experimental and numerical simulations for different welded samples.

To validate the model, the strain distributions obtained from experimental results and FEM simulations were compared. Figure 12 shows a comparison of the local strain for the experimental results and numerical analysis. The simulated distribution matched reasonably well, and it was seen that major plastic strain had taken place only in the softened HAZ (Fig. 13). For the simulations, the major strain values were calculated at the Gauss point and then extrapolated to the nodes, which had a high density in the softened HAZ. However, in the experimental specimen, the softened HAZ is contained within the span of only one circular grid point, and only one major strain value was obtained. In both experimental and numerical results, the major plastic strain is less than 8% in both the hardened zone and base metal, while in the case of the softened zone it is above 35%. The fusion zone and base metal in both the numerical and experimental distribution did not experience significant plastic deformation. Strain was localized in the softened zone, resulting in a final fracture.

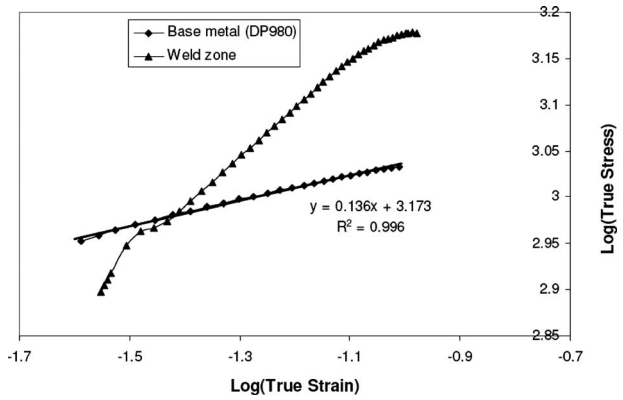

Fig. 7 Log true stress–log true strain curve obtained from the experiment for base metal (DP980) and weld zone

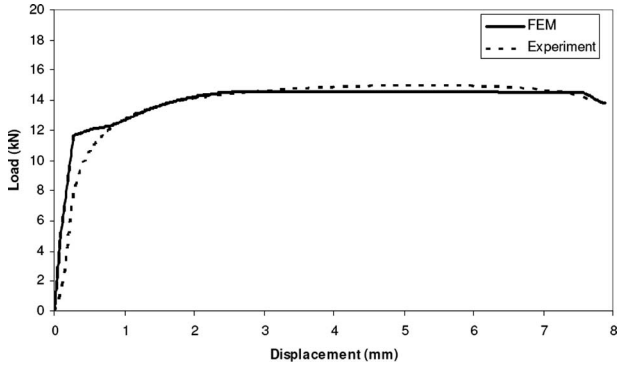

Fig. 8 Comparison of load-elongation curves obtained from experiment and numerical simulation for DP980 steel

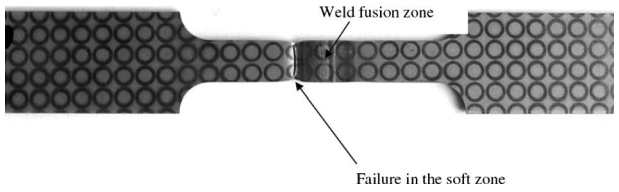

Fig. 10 Localized failure in the softened zone during tensile testing of transverse welded specimens (diode laser weld)

Table 4 Simulated *K*- and *n*-values of the softened zone as compared with those of the base metal

Properties	Base metal	Softened zone Nd:YAG laser	Softened zone Diode laser
n-value	0.14	0.17	0.19
K-value (MPa)	1510	1408	1290

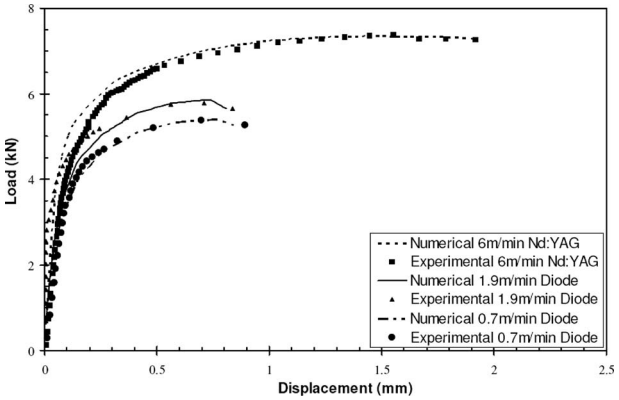

Fig. 11 Comparison of experimental and numerical results for load versus displacement in diode and Nd:YAG laser welds of DP980

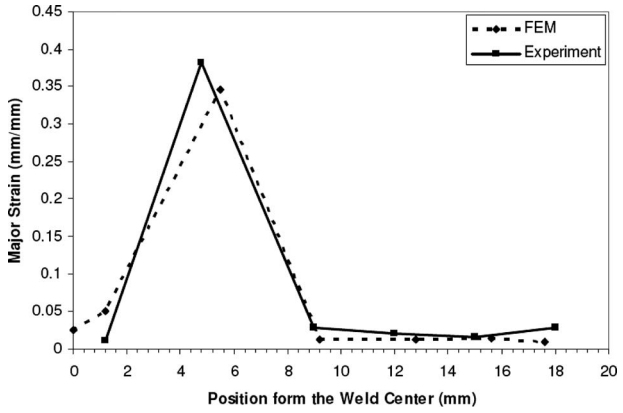

Fig. 12 Comparison of experimental and numerical major strain distributions in the transverse welded tensile specimen (diode laser weld)

4.3 Effect of Softened Zone Material Properties and the Softened Zone Width on the Overall Strength and Elongation. The effects of both material properties and size of the softened zone were studied individually. Tabor estimated that the best correlation between Vickers hardness, H_V, and the flow stress occurs at a strain of 8% as follows [29]:

$$H_V = C\sigma_{0.08} \tag{11}$$

where C is a material constant.

In the work hardening region, the stress-strain curves follow Holloman's equation,

$$\sigma = K\varepsilon_p^n \tag{12}$$

where ε_p is the plastic deformation, K is the strength coefficient, and n is the hardening exponent.

For $\varepsilon = 0.08$ the flow stress should be

$$\sigma_{0.08} = K(\varepsilon_{p,0.08})^n \tag{13}$$

where $\varepsilon_{p,0.08} = 0.08 - \varepsilon_e$, with ε_e being the elastic strain.

From Eqs. (11) and (13) the relation between hardness and strength coefficients is obtained,

$$H_v = CK(\varepsilon_{p,0.08})^n \tag{14}$$

In the next simulation experiments, different softened zone K values (1510 MPa, 1450 MPa, 1410 MPa, 1370 MPa, and 1300 MPa) were used to indirectly vary the hardness of this region while keeping the width of the softened zone constant at 0.5 mm. Figure 14 shows the effect of the softened HAZ strength on the maximum load and displacement of the transverse weld uniaxial tensile test sample. It was found that with decreasing strength (hardness) of the softened zone, the overall load bearing capacity of the welded joint decreased along with the overall displacement.

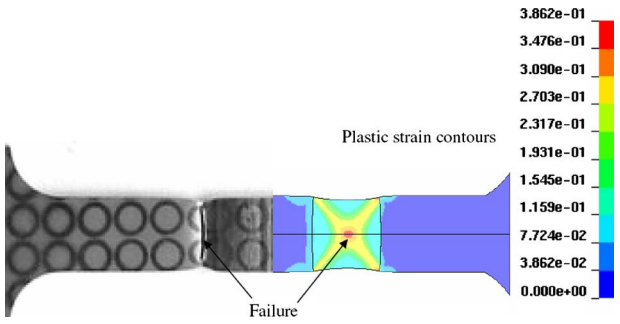

Fig. 13 Strain localization in the softened zone observed in both experiment and FEM simulation

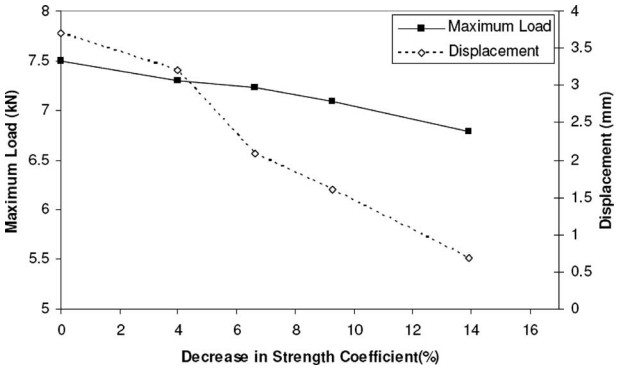

Fig. 14 Simulated maximum load and displacement with respect to the decrease in the softened zone strength for a welded sample with a 0.5 mm softened zone width of HAZ

Figures 15 and 16 show the plastic strain contours for two different softened zone strengths at different times during deformation. It was seen that in the case of the lower strength coefficient ($K = 1300$), there was no uniform strain distribution and strain localization took place in the softened HAZ. However, in the case of the higher strength coefficient ($K = 1450$), the strength of the softened zone increased with strain hardening, which in turn arrested strain localization and resulted in a more uniform distribution in

Fig. 15 Plastic strain contours in the different weld zones for softened zone strengths of (*a*) 1300 MPa and (*b*) 1450 MPa at time=0.1996 s of deformation

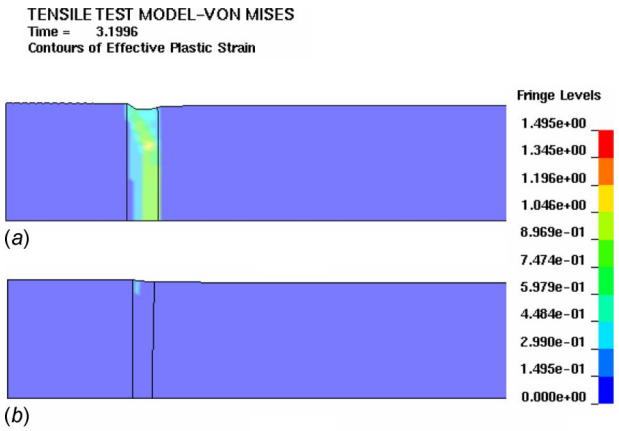

Fig. 16 Plastic strain contours in the different weld zones for softened zone strengths of (*a*) 1300 MPa and (*b*) 1450 MPa at time=3.1996 s of deformation

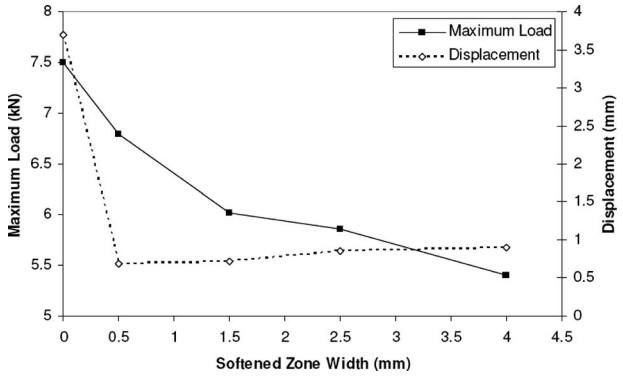

Fig. 17 Simulated maximum load and displacement with respect to the softened zone width (with softened zone strength of 1300 MPa) of HAZ

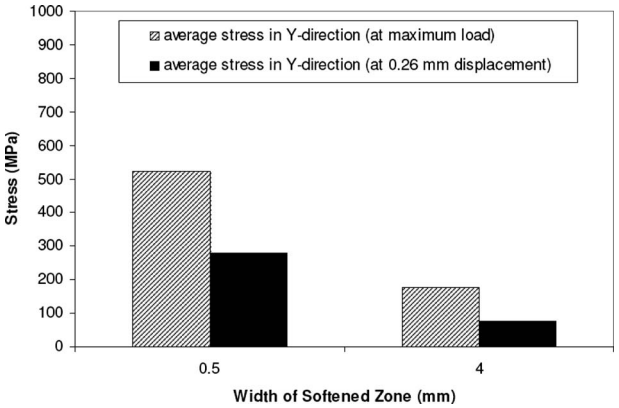

Fig. 19 Comparison of *Y*-stress developed in the welded specimen

the base metal. Thus, premature failure of the specimen in the softened zone was avoided, increasing the overall ductility of the welded tensile specimen.

The width of the softened HAZ was then varied (0 mm, 0.5 mm, 1.5 mm, 2.5 mm, and 4.0 mm), while the strength coefficient was held constant at 1300 MPa. Figure 17 shows the effect of the softened zone width on the maximum load and ductility of the transverse welded specimen. It was found that the load bearing capacity and ductility decreased sharply as soon as the width of the softened HAZ increased above zero (i.e., no softening). With further increase in the softened zone width, the maximum load decreased, but the displacement was nearly constant. Figure 18 shows stress contours in the *Y*-direction (*Y*-stress) developed within the softened zone during deformation. In the hardened zone and the base metal, there was zero *Y*-stress component. The stress in the softened zone changed from a uniaxial to a biaxial stress state, but the hardened zone and the base metal remained in a uniaxial stress state. Deformation was localized in the softened HAZ, and due to the transverse strain component, the width of the sample tended to decrease. The adjacent regions (base metal and hardened zone) resisted the transverse strain in the softened zone, which produced constraint force and stress in the *Y*-direction (Fig. 18).

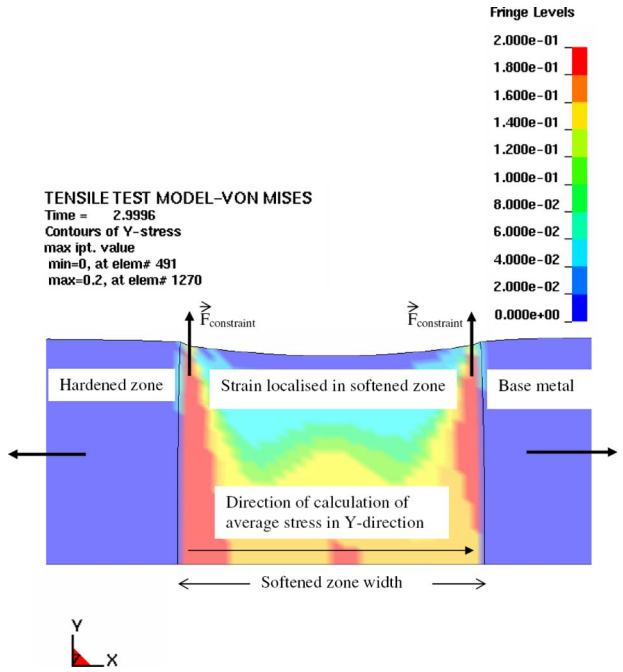

Fig. 18 *Y*-stress distribution (in GPa) in the softened zone (of 4 mm in width) due to the development of constraint force during deformation

The magnitude of the stress component depended on the softened zone width. Figure 19 shows that this *Y*-component decreased as the softened zone width increased from 0.5 mm to 4.0 mm. The hydrostatic stress (mean stress) component, $(1/3)\sigma_{ii}$, within the softened zone increased with increasing *Y*-stress component. Hence, a relatively larger tensile force was required to deform the thinner softened HAZ and overcome the higher hydrostatic stress component. The hydrostatic stress component, however, does not cause plastic deformation. It was found that the strength of the welded specimen with a very narrow softened zone width was close to the base metal.

The simulation results show that both the softened zone size and the hardness (strength) have a significant influence on the load bearing capacity of the welded blank. In terms of ductility, the overall elongation of the sample decreases with decreasing strength in the softened zone; however, it is relatively unaffected by increasing softened zone width. In real welds, the severity of softening and the softened zone width both increase with increasing heat input. As a result, these two factors must be considered simultaneously. Figure. 11 shows the effects of heat input on the strength and ductility of the transverse weld tensile sample. Both the maximum load and the displacement were significantly lower in the high heat input diode welds than in the low heat input Nd:YAG welds. The diode welds exhibited a wider and softer HAZ than the Nd:YAG welds. When the weld speed was decreased from 1.9 m/min to 0.7 m/min with the diode laser, the width of the softened HAZ increased; however, the hardness in the softened HAZ was nearly constant. At high heat inputs, the martensite was fully tempered and the hardness does not change with increasing heat input. As a result, the maximum load of the tensile samples decreased with increasing heat input; however, the sample elongation was relatively unaffected.

5 Conclusions

The transverse tensile strength and ductility of laser welded blanks are significantly degraded in a DP980 steel, which exhibits softening in the HAZ. When strained to failure, fracture is coincident with the location of the softened HAZ. The weld strength and ductility are affected by the width and severity of the softened region, which are functions of the heat input and vary with changes in laser type, power, and speed.

The mechanical properties in the softened HAZ are difficult to measure experimentally; however, they can be assessed by a comparison of experimental results with simulated uniaxial tensile tests.

A finite element analysis shows that the strength of the joint decreases significantly with the formation of a softened zone. As the strength of the softened zone decreases, the strength of the joint decreases as well.

Numerical results show that increasing the width of the softened zone with a constant strength results in a decrease in the overall joint strength, while the elongation is unaffected. This is a result of increased hydrostatic constraint stress with decreasing soft zone width.

References

[1] Irving, B., 1991, "Blank Welding Forces Automakers to Sit Up and Take Notice," Weld. J. (Miami, FL, U.S.), **70**(9), pp. 39–45.

[2] Irving, B., 1995, "Welding Tailored Blanks is Hot Issue for Automakers," Weld. J. (Miami, FL, U.S.), **74**(8), pp. 49–52.

[3] Bleck, W., 1996, "Cold-Rolled, High-Strength Steels for Auto Applications," J. Met., **48**, pp. 26–30.

[4] Uchihara, M., and Fukui, K., 2003, "Tailored Blanks of High Strength Steels-Comparison of Welding Processes," SAE Technical Paper Series No. 2003-01-2829.

[5] Chan, S. M., Chan, L. C., and Lee, T. C., 2003, "Tailored Welded Blanks of Different Thickness Ratios Effects on Forming Limit Diagrams," J. Mater. Process. Technol., **132**, pp. 95–101.

[6] Herfurth, H. J., and Ehlers, B., 2000, "Increased Performance Broadens Processing Capabilities of High Power Diode Lasers," *Proceedings of the 19th International Congress-ICALEO*, Dearborn, MI, Oct. 2–5, pp. 9–18.

[7] Bocos, J. L., Zubiri, F., Garciandia, F., Pena, J., Cortiella, A., Berrueta, J. M., and Zapirain, F., 2005, "Application of the Diode Laser to Welding on Tailored Blanks," Weld. Int., **19**(7), pp. 539–543.

[8] Breakiron, B., and Fekete, J. R., 2005, "Formability Analysis of High Strength Steel Laser Welded Blanks," SAE Technical Paper Series No. 2005-01-1326.

[9] Hartley, B., and Ono, M., 2002, "Laser Weldability of Dual Phase Steels in Tailored Blank Applications," SAE Technical Paper Series No. 2002-01-0150.

[10] Sreenivasan, N., Xia, M., Lawson, S., and Zhou, Y., 2008, "Effects of Laser Welding on Formability of DP980 Steel," ASME J. Eng. Mater. Technol., to be published.

[11] Shao, H., Gould, J., and Albright, C., 2007, "Laser Blank Welding High-Strength Steels," Metall. Mater. Trans. B, **38**, pp. 321–331.

[12] Tomokiyo, T., Taniguchi, H., Okamoto, R., Miyagi, T., and Furusako, S., 2006, "Effect of HAZ Softening on the Erichsen Value of Tailored Blanks," SAE Technical Paper Series No. 2006-05-0140.

[13] Xia, M., Sreenivasan, N., Lawson, S., and Zhou, Y., 2007, "A Comparative Study of Formability of Diode Laser Welds in DP980 and HSLA Steels," ASME J. Eng. Mater. Technol., **129**, pp. 446–452.

[14] Nakagawa, N., Ikura, S., Natsumi, F., and Iwata, N., 1993, "Finite Element Simulation of Stamping a Laser-Welded Blank," SAE Technical Paper Series No. 930522.

[15] Saunders, F. I., and Wagoner, R. H., 1996, "Forming of Tailor-Welded Blanks," Metall. Mater. Trans. A, **27**, pp. 2605–2616.

[16] Ghoo, B. Y., Keum, Y. T., and Kim, Y. S., 2001, "Evaluation of the Mechanical Properties of Welded Metal in Tailored Steel Sheet Welded by CO2 Laser," J. Mater. Process. Technol., **113**, pp. 692–698.

[17] Dry, D., Wadell, W., and Owen, D. R. J., 2002, "Determination of Laser Weld Properties for Finite Element Analysis of Laser Welded Tailored Blanks," Sci. Technol. Weld. Joining, **7**(1), pp. 11–18.

[18] Rodrigues, D. M., Menezes, L. F., Loureiro, A., and Fernandes, J. V., 2004, "Numerical Study of the Plastic Behaviour in Tension of Welds in High Strength Steels," Int. J. Plast., **20**, pp. 1–18.

[19] Mellor, P. B., 1981, "Sheet Metal Forming," Int. Met. Rev., **1**, pp. 1–20.

[20] ASTM E8-01, 2003, "Standard Test Methods for Tension Testing of Metallic Materials," *Annual Book of ASTM Standards*, ASTM, Philadelphia.

[21] Panda, S. K., Ravi Kumar, D., Kumar, H., and Nath, A. K., 2007, "Characterization of Tensile Properties of Tailor Welded IF Steel Sheets and Their Formability in Stretch Forming," J. Mater. Process. Technol., **183**, pp. 321–332.

[22] Abdullah, K., Wild, P. M., Jeswiet, J. J., and Ghasempoor, A., 2001, "Tensile Testing of Weld Deformation Properties in Similiar Gage Tailor Welded Blanks Using the Rule of Mixtures," J. Mater. Process. Technol., **112**, pp. 91–97.

[23] Smerd, R., Winkler, S., and Worswick, M., 2005, "High Rate Tensile Testing of Automotive Aluminum Alloy Sheet," Int. J. Impact Eng., **32**, pp. 541–560.

[24] Hallquist, J. O., 2003, LS-DYNA User's Manual, LSTC, Inc.

[25] HYPERMESH 7.0 User's Manual, Altair Computing, Inc.

[26] Johnson, W., and Mellor, P. B., 1975, *Engineering Plasticity*, Van Nostrand Reinhold, London.

[27] Dieter, G. E., 1988, *Mechanical Metallurgy*, McGraw-Hill, Singapore.

[28] Akbarpour, M. R., and Ekrami, A., 2008, "Effect of Ferrite Volume Fraction on Work Hardening Behavior of High Bainite Dual Phase (DP) Steels," Mater. Sci. Eng., A, **477**, pp. 306–310.

[29] Tabor, D., 1951, *The Hardness of Metals*, Oxford University Press, New York.